Towards the Noise Reduction of Piezoelectrical-Driven Synthetic Jet Actuators

Mark Jabbal[a,*], Jonne Jeyalingam[b]

[a] *Faculty of Engineering, University of Nottingham, NG7 2RD, UK*
[b] *College of Engineering, Design and Physical Sciences, Brunel University London, UB8 3PH, UK*

Abstract
This work details an experimental investigation aimed at reducing the noise output of piezoelectrical-driven synthetic jet actuators while minimizing peak jet velocity reduction. The study considers double-chamber actuator for anti-phase noise suppression and lobed orifice as a method to enhance jet turbulent mixing to suppress jet noise. The study involved the design, manufacture and bench test of interchangeable actuator hardware. Hot-wire anemometry and microphone recordings were employed to acquire velocity and sound pressure level measurements respectively across a range of excitation frequencies for a fixed diaphragm clamping and input voltage. The data analysis indicated a 26% noise reduction (16 dB) from operating a single-chamber, round orifice actuator to a double-chamber, lobed orifice one at the synthetic jet resonant frequency. Results also showed there was a small reduction in peak jet velocity of 7% (~3 m/s) between these two cases based on orifices of the same discharge area. The electrical-to-fluidic power conversion efficiency of the double-chamber actuator was found to be 15% for both orifice types at the resonant frequency; approximately double the efficiency of a single-chamber actuator.

Keywords
Synthetic jet actuator; noise reduction; dipole, lobed orifice

1. Introduction

A synthetic jet actuator (SJA) is a zero-net mass flux device that negates the need for a network of pneumatic ducts. Instead, it generates fluidic power through an orifice on one side of a chamber using an oscillating diaphragm on the opposite side. In the case of a piezoceramic diaphragm, an input electrical supply is required to create the oscillatory motion. The momentum that a SJA imparts to a fluid flow can delay boundary layer separation, which could be used to improve the effectiveness of aircraft high-lift and control surfaces [1], [2].

One of the major limitations of a SJA for aircraft application is its high noise output generated from the motion of the diaphragm and jet stream mixing with the atmosphere. Unfortunately SJA effectiveness often dictates operation at the actuator resonant frequency to maximise authority, which coincides with the highest tonal noise output. Since SJAs generate discrete high-momentum jets, then to introduce significant effects in large scale flow they must be used in large numbers, e.g. in arrays along the span of the wing. Although there has been much research on optimising SJAs for peak jet velocity, there has been far fewer studies on minimising SJA noise.

Table 1 summarises noise reduction methods employed for SJAs. It was observed by Arik [3] that the sound pressure level (SPL) from a SJA can be as high as 73 dB when operating at a resonant frequency, f=3.6 kHz for a peak jet velocity, U_{peak}=90 m/s out of a round orifice of diameter, d=1 mm. Noise abatement using passive mufflers was shown to reduce SPL to 30 dB, but at a cost of significantly increasing the actuator volume to a level that is unviable for aircraft implementation. Lasance *et al*. investigated the influence of pipe length [4] and actuator power [5] on SJA noise (the SJA featured a cavity backed with a vibrating loudspeaker and two adjacent protruding pipes for the jet outflow). As might be expected, SPL increased with power however the influence of pipe length was less clear with reduced noise reported for increasing pipe length at d=3 mm and the reverse trend at d=4 mm. Although the two pipes were in an acoustic dipole, no noise reduction results of this arrangement were reported relative to a single monopole pipe. Bhapkar *et al*. investigated the influence of orifice diameter [6] and orifice height [7] on SJA noise. SPL was reduced for smaller orifice diameters and smaller orifice height, i.e. thinner orifice plates. Mangate and Chaudhari [8] recorded SJA noise as high as 68 dB for an operating frequency of 0.4 kHz out of a 8 mm round orifice. Noise was reduced to 64 dB and 57 dB respectively for diamond and oval orifices of equivalent diameters.

* Corresponding author. E-mail address: mark_jabbal@hotmail.com

The aforementioned studies are all focused on using SJAs to enhance heat transfer for thermal cooling applications. With the exception of [3], the rest incorporate orifice diameters which are an order of magnitude larger or orifice lengths that are upto two orders of magnitude larger than those required for aircraft separation control. In addition, actuation frequencies are an order of magnitude lower and hence peak exit velocities are much lower than those required for separation control. The aim of the present work is to explore methods of reducing the noise generated by piezoelectrical-driven SJAs without decreasing peak jet velocity relative to a round orifice SJA baseline. Emphasis is given to such methods which are conducive for use in an aircraft separation control setting.

Table 1. Noise reduction methods employed for synthetic jet actuators

Study	Orifice	*d* (mm)	*f* (kHz)	U_{peak} (m/s)	SPL (dB)	Noise abatement	SPL (dB)
Arik [3]	Round hole	1	3.6	90	73	Passive muffler	30
Lasance *et al.* [4]	Round hole	3	0.11	6.5	43.1 (l=30 mm)	Pipe length	41.5 (l=90 mm) 36.9 (l=120mm)
		4	0.11	6.5	49 (l=120 mm)		46.4 (l=30 mm) 48.1 (l=90 mm)
Lasance *et al.* [5]	Round hole	4 8	0.03 0.08	… …	37 (P=1 W) 52 (P=0.3 W)	SJA power	32 (P=0.4 W) 46 (P=0.1 W)
Bhapkar *et al*. [6]	Round hole	14	0.1	21	58	Orifice diameter	48 (d=8 mm) 53 (d=10 mm) 55 (d=12 mm)
Bhapkar *et al*. [7]	Elliptical hole	12	0.1	21	58 (h=5 mm)	Orifice height	54 (h=2 mm)
Mangate & Choudhari [8]	Round hole	8	0.4	…	68	Orifice shape	57 (oval) 64 (diamond)

A SJA has two main sources of noise: jet noise and diaphragm noise. Jet noise is generated from the turbulent mixing of the flow exiting the orifice with the surrounding air. A potential core is formed just aft of the orifice exit containing laminar flow. The length of the core is typically 4 to 5 times the diameter of the orifice [9], [10]. The mixing of the synthetic jet with the ambient air occurs at a region around the potential core. Further downstream of the orifice exit, the jet spreads out at a wider angle, forming a fully-developed flow region. The vortex rings formed at the edges of the orifice increase in size and decrease in velocity as they propagate away from the SJA. The frequency of sound generated is inversely proportional to the size of the vortex rings. This means that high frequency sound is generated close to the orifice and low frequency sound derives from the fully-developed jet far from the orifice exit [11]. The continuously vibrating diaphragm creates acoustic waves inside the chamber, which bounce between the walls and finally escape through the orifice exit in to the external ambient [12].

A double-chamber SJA consists of two chambers and two orifices. The two orifice plates are located perpendicular to the shared oscillating diaphragm (Fig. 1). The double-chamber SJA design has the ability to offer reduced noise output. Firstly, the presence of a second chamber on the other side of the diaphragm acts as a sound barrier preventing sound waves from propagating in to the atmosphere. It is also possible that the two orifices of a double-chamber SJA can act as a fluid mechanical dipole source. The orifice of a SJA can be characterized as a monopole source of sound (Fig. 2a). This source radiates sound in all directions; in this case, jet noise is radiated to the atmosphere. A dipole source is the close placement of two monopole sources of equal strength and exactly opposite phase [13]. When one source produces a net outflow, the other one produces an exactly opposite inflow. In contrast to a single monopole, the net fluid flux is zero. However, a net fluctuating force is produced because of the 180° out-of-phase oscillation. In the case of a double-chamber SJA, the two orifice plates have the same dimensions (orifice diameter and depth) and are situated close to each other. As the diaphragm oscillates back and forth, flow from one orifice is exhaled while at the same time ambient air is inhaled in the other orifice. This indicates that the

two orifices produce a net fluctuating source and are 180° out-of-phase. The propagating sound waves produced interact with each other and cancel out at 90° and 270° from the sound sources (Fig. 2b).

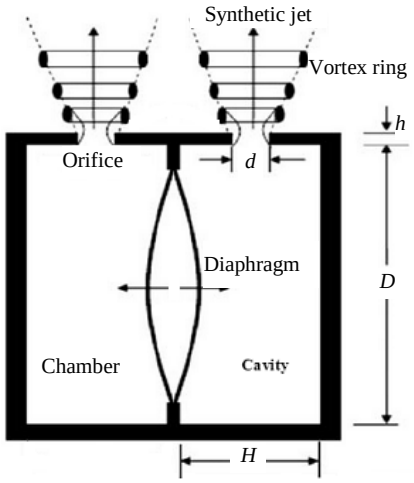

Figure 1. Double-chamber SJA

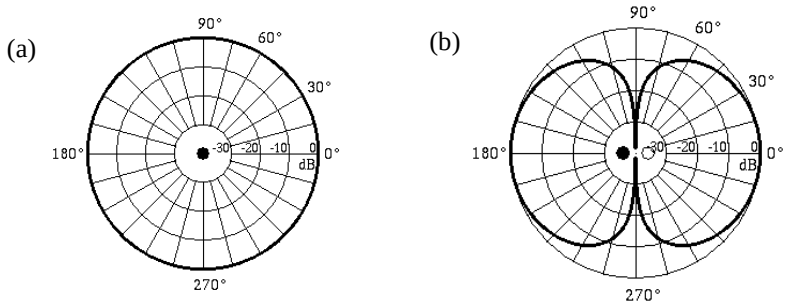

Figure 2. (a) monopole source – sound radiates in all directions, (b) dipole source – sound waves cancel out at 90 and 270 degrees from the sources [14]

There have been several nozzle design modifications devised in an effort to reduce jet exhaust noise. Research has been conducted by the aviation industry in order to specifically reduce the noise produced by aircraft jet engines. Such design modifications include chevron and corrugated nozzles. These nozzles reduce jet noise by inducing streamwise vorticity along the shear boundary layer in the jet flow. The added vorticity causes smoother mixing of the jet core with the ambient air, reducing the rapid pressure fluctuations responsible for jet noise. Enhanced mixing slightly increases the high frequency noise ranging from 7.5 kHz to 30 kHz [15]. However due to the breakdown of the larger scale turbulence into small scale, this mixing reduces the low frequency noise (below 7.5 kHz) resulting in reduction of the overall sound pressure level [16].

Chevron nozzles reduce exhaust noise with minimal penalty on performance. The chevron count and penetration is a primary factor in controlling the compromise between low-frequency reduction and high-frequency sound pressure level (SPL) augmentation. It has been proven experimentally [17] that a higher chevron count with a lower level of penetration and zero degree taper, yields the maximum noise reduction for low and medium nozzle pressure ratios. Specifically, a chevron nozzle with eight lobed chevrons reduces jet noise by 8 dB.

For a SJA, the use of lobed orifices (also known as corrugated, crimped or daisy orifices) is more practical for aircraft applications due to the shape modification being in the plane of the orifice exit rather than out-of-plane, as is the case with chevrons on an a nacelle at the engine exhaust. It is shown for a continuous jet that an increase in the lobe amplitude leads to noise reduction in the far field [15]. Similar to chevron nozzles, there is a small increase of

noise in the high frequency region but a decrease of noise level in the low frequency regions; typically 2.3 dB reduction for frequencies up to 5 kHz compared with a round orifice of the same area. The lobed jet mixing flow has larger intensive mixing regions in the near field of the jet compared with its non-lobed counterpart. The unique geometry of the lobes generates large scale streamwise vortices of alternating sign, thereby increasing the mixing efficiency [18], [19]. Consequently, the length of the potential core in the lobed jet mixing flow is 1/4 to 1/6 of that in the conventional round jet flow. The performance of these nozzles depends on the configuration of the geometric parameters such as the number of lobes, their angle as well as their shape [20].

2. Experimental Approach

2.1 Actuator Design

The velocity of the exhaled jet has a great impact on SJA performance with regards to their ability to control boundary layer separation on high-lift surfaces. Peak velocities of piezoelectrically-actuated synthetic jets of the order of 80–120 m/s have been attained [21], [22]. As a rule of thumb, the orifice diameter should scale as a percentage of the boundary layer height in which it's embedded – typically equivalent to that of a sub boundary layer vortex generator (SBLVG) height scaling [21], [23]. For this work the orifice diameter, d, is set to 1 mm. The orifice height can strongly impact the peak velocity of the ensuing synthetic jet. An orifice with too large a height will tend to have a large damping effect on the airflow, resulting in a limited peak velocity. On the other hand, if the orifice neck is too short, the jet will not accelerate sufficiently to produce the desired peak velocities. The optimised height should be approximately 1.25 times the orifice diameter [24]; the orifice height, h, was constrained to $1.5d$ (i.e. h = 1.5 mm). The chamber diameter is defined by the diameter of the diaphragm. The diaphragm used consists of a polycrystalline piezoceramic (PZT-5A) disc bonded to a 27 mm brass plate (OBO-TE27241-16) with a total thickness of 0.45 mm. The diaphragm has to be held firmly in the chamber by being clamped uniformly 1 mm from its perimeter. Consequently the diameter of the chamber, D, is set to 25 mm.

The peak velocity of a SJA is inversely proportional to the depth of its chamber [24], [25]. However for a double-chamber SJA, the chamber depth is restricted by the separation distance between the two orifices. As the jets will operate in anti-phase there is the risk that the jet being exhaled from one SJA could be inhaled during the suction stroke of the adjacent SJA if the orifices are too close together. It was therefore decided to position the orifices $5d$ apart (5 mm); this distance is also the limit of the range of optimised spacing for separation control established from experiments with arrays of SBLVGs and fluidic jets [26], [27], [28]. The orifice is situated at the middle of each chamber to ensure peak velocity output. Taking into account both aforementioned requirements and the thickness of the clamped part of the diaphragm (0.22 mm), the depth of each chamber, H, in the double configuration is 4.78 mm.

A SJA device acts like a two-degree of freedom forced mass-spring-damper system with two characteristic resonance frequencies [29], [30], [31], [32], which are related to, but not necessarily the same as, the theoretical Helmholtz resonant frequency and mechanical resonant frequency. Helmholtz resonance occurs as a result of a dynamic exchange of kinetic energy of the fluid in the orifice with the potential (pressure) energy of the fluid in the chamber. A double-chamber SJA effectively has a pair of resonators located close to each other producing oscillating flows which are in anti-phase. Due to the relatively small separation distance between the two resonators, the peak frequency response of both orifices is expected to increase. As previously shown [33], a spanwise row of resonators increases the resonating frequency of a system in comparison to a single resonator's frequency. This effect is observed as the two orifice resonant frequencies are coupled into a new higher frequency by the fluid mechanical interaction. The theoretical Helmholtz resonance [29], f_H, is given by Eq. (1)

$$f_H = \frac{a}{2\pi}\sqrt{\left(\frac{d}{D}\right)^2 \frac{1}{Hh}} \tag{1}$$

Where a is the speed of sound. From what is known of the single-chamber SJA Helmoltz resonance (f_H = 812 Hz) and aforementioned fluid mechanical coupling between adjacent SJAs, it can be expected that the resonant frequency associated with f_H will be higher for the double-chamber configuration.

The natural or mechanical resonant frequency of the diaphragm often provides the greatest peak velocity output and thus tends to be more influential than the Helmholtz resonance. It is dependent on the geometric and material properties of the diaphragm. The natural frequency of a circular plate [22], f_D, akin to a SJA diaphragm is given by Eq. (2)

$$f_D = \frac{k^2 t_D}{2\pi r_D^2}\left(\sqrt{\frac{E(1-2\xi)}{12\rho(1-\nu^2)}}\right) \tag{2}$$

Where r_D and t_D are the diaphragm radius and thickness respectively; E, ρ and ν represent the diaphragm material properties (Young's modulus, density and Poisson's ratio, respectively); ζ is the damping coefficient and k^2 is a dimensionless frequency parameter, which is primarily a function of the diaphragm boundary conditions [34]. Table 2 summarises the diaphragm characteristics. The value of the natural frequency of the SJA diaphragm, f_D = 1960 Hz.

Table 2. SJA diaphragm characteristics

r_D (mm)	t_D (mm)	E (GPa)	ρ (kg/m^3)	ν	k^2	ζ
13.5	0.45	103	8450	0.33	4.98	0.06

The SJA design is shown in Fig. 3. It was necessary to design the actuator in such a way that the orifice plates are interchangeable to facilitate lobed and round orifice testing.

(a)

(b)

(c)

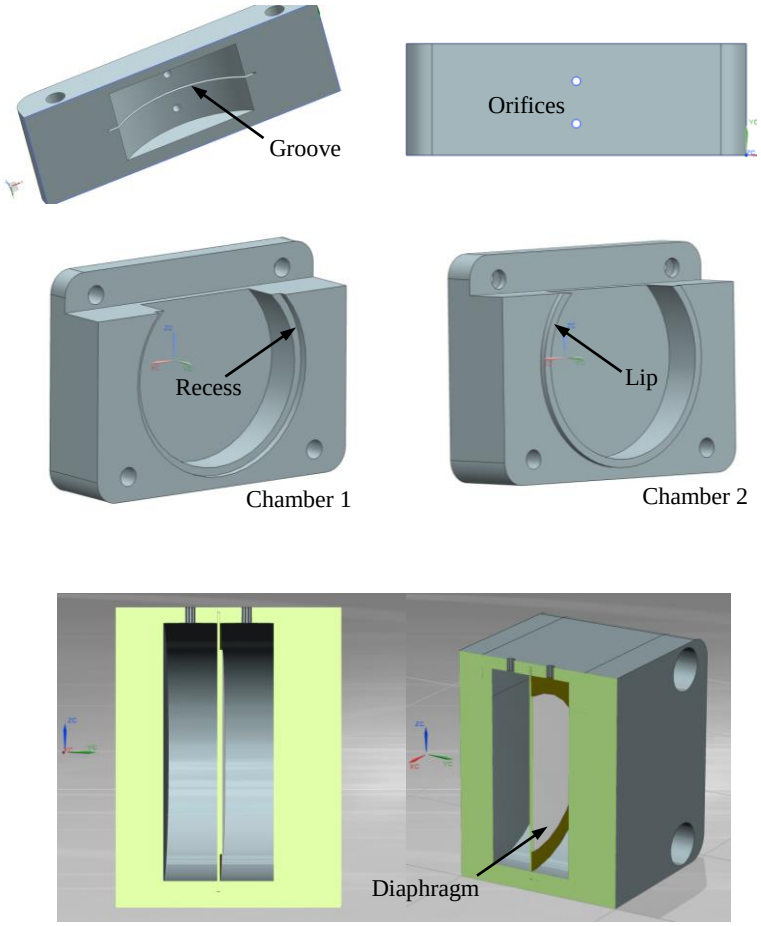

Figure 3. (a) baseline orifice plate design; (b) chamber design; (c) cross-sectional view of SJA

The maximum thickness of the orifice plate is 5 mm and it possesses a small groove located between the two orifices (Fig. 3a). The purpose of the groove is to locate the diaphragm. The double-chamber design consists of Chamber 1 and Chamber 2 (Fig. 3b). Chamber 1 has a small recess (1 mm depth), where the diaphragm is positioned. Chamber 2 has a small lip (0.78 mm height), which when assembled with Chamber 1 will provide a compressive load on the diaphragm.

A lobed orifice was achieved by designing a dodecagon, as shown in Fig. 4a. With 12 lines of symmetry and rotational symmetry of order 12, all sides are of equal length and all internal angles equal to 150°. Six lobes were designed round the dodecagon in a sinusoidal manner and have the same radius of 0.5 mm (Fig. 4b). The area and hence discharge rate of the lobed orifice is designed to correspond to the round orifice. The 12 sides of the dodecagon have an arc length of 0.26 mm giving an orifice area of 7.6×10^{-7} m^2 (this is equivalent to 97% of the round orifice area, $A = 7.85\times10^{-7}$ m^2). The two interchangeable orifice plates were printed using a high grade stainless steel, 316L (Fig. 4c).

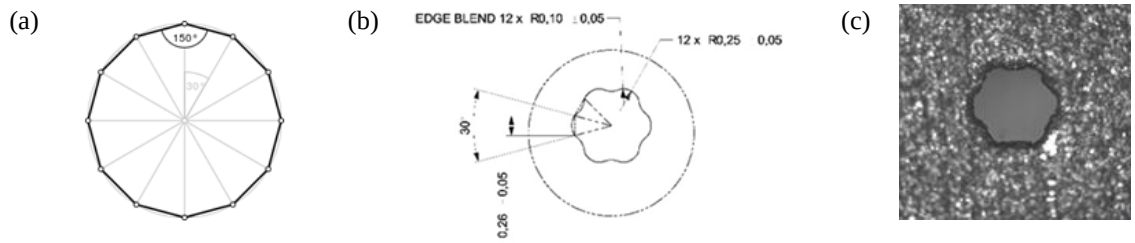

Figure 4. (a) Schematic of lobed orifice set up; (b) lobed orifice dimensions (in millimetres); (c) magnified image of manufactured lobed orifice

2.2 Test Procedure

2.2.1 Jet Velocity Measurement

The SJA drive components are shown in Fig. 5. A Trek PZD350A high-voltage piezo amplifier with an output voltage range of 0 to ±350V DC or peak AC was used to drive the diaphragm. The voltage signal sent to the PZT disc from the amplifier was controlled by a TTI TG215 2MHz function generator. A fixed sinusoidal voltage waveform was used. Two digital bench multimeters (Model UT801) were connected to the piezo amplifier to provide voltage and current readings. Each SJA was tested with peak-to-peak voltage input, V_{pp} = 100 and 200 V at excitatation frequencies 800 Hz to 3 kHz in increments of 100 Hz. Measurement readings of peak velocity were acquired from a Dantec Dynamic 55P11 single hot wire anemometer sensor probe. The hot-wire probe was positioned 1 mm from the orifice exit using a vertical micrometer.

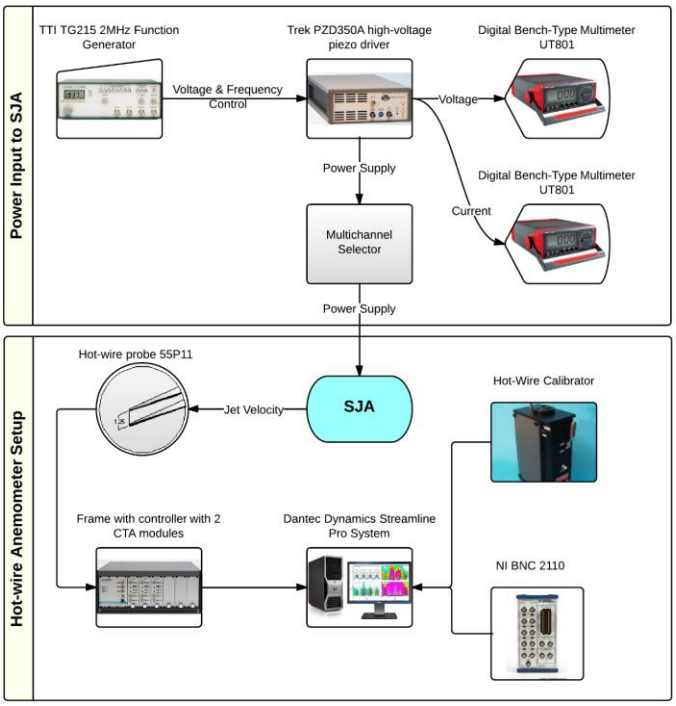

Figure 5. SJA jet velocity measurement setup

2.2.2 Power Conversion Efficiency Measurement

The power supplied to a SJA can be considered as electric energy input, $\dot{E}$. Some of this energy is stored as electrical potential energy because of the electric capacitance of the PZT diaphragm, which is denoted as $\dot{C}$. The remaining energy is converted to mechanical energy along with energy loss. The mechanical energy of the actuator can be considered as the vibration of the piezoelectric diaphragm plus the synthetic jet exiting the orifice. It is necessary to determine the electric-to-fluidic power conversion efficiency of the SJA and so the mechanical energy of the diaphragm due to vibration is not considered. It is assumed that the static pressure and specific volume of air at the orifice are the same as the ambient. Therefore, the energy of airflow exiting the orifice is equal to its kinetic energy, $\dot{F}$. The energy loss of the SJA is incurred due to the deflection of the diaphragm as well as some energy loss in airflow prior to exiting the orifice. The total energy loss is represented by $\dot{L}$. Figure 6a shows the rate of input and output energy conversion of a single chamber SJA. For double-chamber SJAs (Fig. 6b), the flow power will be higher due to the ejection of two synthetic jets for the same power input. The efficiency of energy conversion for synthetic jets is the ratio of the output and input energy given by Eq. 3

$$\eta = \frac{\dot{F}}{\dot{E}} \tag{3}$$

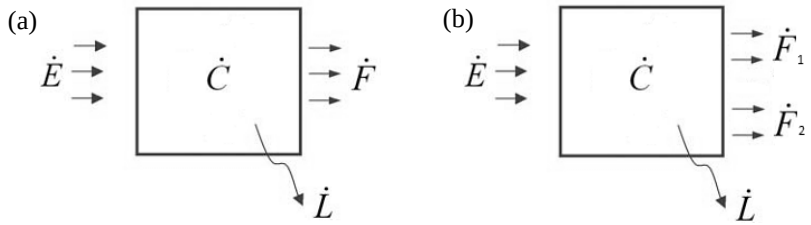

Figure 6. Energy conversion comparison between (a) single- and (b) double-chamber SJA

To calculate efficiency it is necessary to determine the flow power. The airflow power for a single chamber SJA [35] is given by

$$\dot{F} = \frac{1}{2}\rho A U^3 \tag{4}$$

Where A is the SJA orifice area, ρ is the density of air and U is the synthetic jet velocity. For a double-chamber configuration with two synthetic jets the airflow power is given by

$$\dot{F} = \dot{F}_1 + \dot{F}_2 \tag{5}$$

The power input applied to the piezoelectric diaphragm depends on the voltage amplitude. Due to the electrical capacitance of the diaphragm, there is a phase angle difference between the voltage and current. Because of that, the current signal has a time delay that varies over a range of frequencies. The phase angle is given by

$$\phi = 2\pi f \Delta t \tag{6}$$

The instantaneous true power input is calculated as

$$\dot{E} = V_{peak} I_{peak} \sin(2\pi f t) \sin(2\pi f t + \phi) \tag{7}$$

Where V_{peak} and I_{peak} is the peak voltage and peak current respectively, f is the excitation frequency and t is the instantaneous time.

Since the experimental velocity measurements were compared at peak velocities, U_{peak}, the flow and electrical power are calculated at peak values (F_{peak} and E_{peak} respectively). It is necessary to obtain an expression for the peak electrical power. From trigonometry

$$V_{peak} I_{peak} \sin(2\pi f t) \sin(2\pi f t + \phi) = \frac{1}{2} V_{peak} I_{peak} \left(\cos(\phi) - \cos(4\pi f t + \phi)\right) \tag{8}$$

Equation 8 is a function of time and will give the maximum peak true power when the term $\cos(4\pi f t + \phi) = -1$. The rest of the terms remain constant at a given frequency. Therefore

$$E_{peak} = \frac{1}{2} V_{peak} I_{peak} \left(\cos\phi + 1\right) \tag{9}$$

where E_{peak} is the peak power input and $\cos\phi$ is the power factor, which is equivalent to the phase angle (Eq. 6). The power input was calculated based on Eq. 9; the phase difference between the voltage and current signals was captured using a digital oscilloscope, PicoScope.

2.2.3 Noise Measurement

The SJA noise measurement components are shown in Fig. 7. The microphone set consists of a GRAS 1/4" Type 46BH precision microphone and a 1/4" preamplifier Type 26TC with integrated 3 m cable with a 7-pin LEMO connector. The 46BH precision microphone is usually used for high level acoustic measurements. It's very low sensitivity and wide frequency response make it ideal for the SJA noise experiments where it is expected to acquire measurements of the order of 60-70 dB at the resonant frequencies. A GRAS Power Module Type 12AK is used to power the microphone set. The power module has an output socket which is connected through a BNC cable to National Instrument BNC 2100 for data logging. The filter and gain settings were linear and +50 dB, respectively.

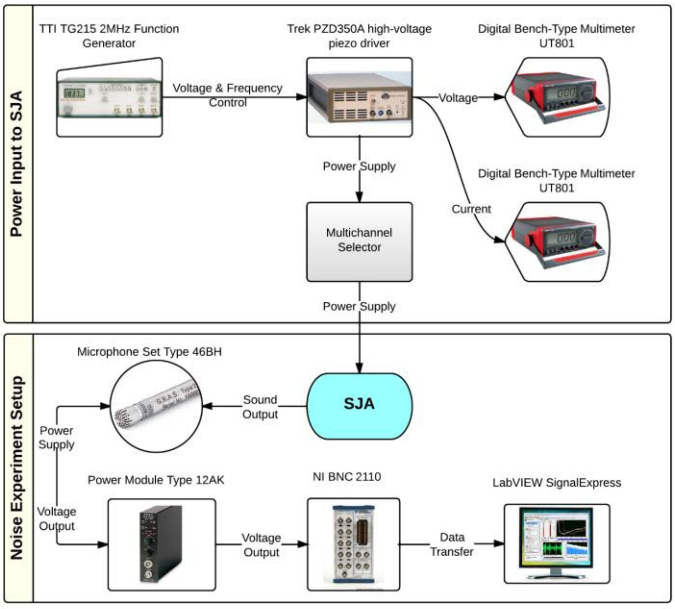

Figure 7. SJA jet noise measurement setup

SJA noise measurements were conducted in a purposely built test rig that simulates an anechoic chamber (Fig. 8). The rig takes the form of a 300 mm cube box of 10 mm thick Perspex. Acoustic panels made from pyramidial polyurethane foam were installed on the inside walls of the test rig. The panels act as sound absorbers to limit the reflection of sound waves made by the SJA inside the chamber. A removable base was necessary for ease of placement of the SJA. The SJA was firmly secured in a vice which is mounted on the centre of the chamber floor. Acoustic foam was also placed between the SJA and vice to eliminate sound due to vibrations transferring from the actuator to the vice. The microphone was placed inside the chamber through an aperture located at the centre of the ceiling and at a distance of 100 mm (100*d*) from the SJA orifice plate. It has been shown by Viswanathan [36] that a distance of at least 35 nozzle diameters ensures measurement in the true far field for jet noise. The microphone was positioned directly above the SJA orifice in both single and double chamber configurations. Test parameters (SJA input voltage and excitation frequency range) for the jet velocity measurements were replicated for the jet noise measurements.

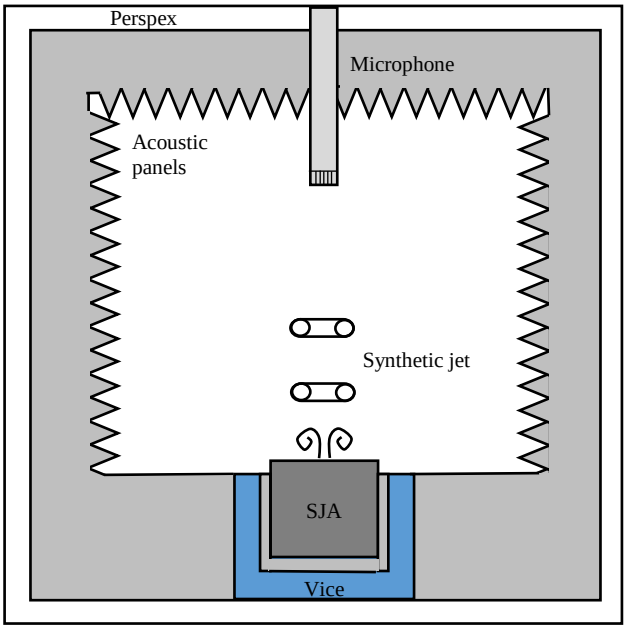

Figure 8. Test rig for SJA noise measurements

The microphone's voltage output values were captured in LabVIEW. The voltage waveform is sinusoidal, therefore to determine the peak sound pressure level at a given frequency, it was necessary to extract the peak voltage amplitude for positive and negative values. The peak-to-peak voltage was used to convert the voltage output into sound pressure level (SPL) of the SJA in decibels by Eq. 10

$$SPL = 20\log_{10}\left(\frac{V_{pp}}{V_{ref}}\right) - \text{mic sensitivity} + \text{calibration input signal} - \text{amp gain} \tag{10}$$

where V_{pp} is the peak-to-peak voltage output of the microphone and V_{ref} is the transform factor of the microphone (mV/Pa). Microphone sensitivity and calibration signal are -66.13 dB re. 1 V/Pa and 114 dB, respectively. The absolute SPL values for each orifice plate were filtered by applying an A-weighted factor in an effort to account for the relative loudness perceived by the human ear. The noise results are therefore presented in units of dBA.

3 Results

3.1 Jet Velocity

3.1.1 Single- and double-chamber comparisons

In order to assess whether there is fluid mechanic interaction between the oscillating flows at the orifices of the double-chamber SJA, Orifice 2 was blocked with tape to simulate a single-chamber SJA. Velocity measurements were taken for Orifice 1 of the round orifice at 100 V_{pp} and the results are shown in Fig 9. It is observed that Orifice 1 behaves in a very similar manner in both double and single chamber configurations. The output peak velocity variation across all frequency responses is less than 5 m/s between the two arrangements. A resonant frequency at 1.7 kHz with a peak jet velocity of 38 m/s is observed. From Fig. 9, it can therefore be reasonably concluded that, in the double-chamber SJA configuration, the two orifices at a distance of 5*d* apart do not have fluid interaction with each other that causes the jet velocity to be diminished. This also corroborates the findings of Greco *et al*. [9], in

which it was shown that twin synthetic jets spaced 5*d* apart showed the same behaviour with respect to the single synthetic jet.

3.1.2 Orifice shape comparisions

It can be seen from Fig. 10a that the velocity output of the two round orifices have a similar trend. A maximum peak jet velocity of 38 m/s and 34 m/s was obtained at 1.7 kHz for Orifice 1 and Orifice 2 respectively. The frequency response is dominated by a single peak at 1.7 kHz, which correlates closely to the theoretical value of diaphragm resonance (1.96 kHz). Figure 10b presents the lobed SJA data. Similarly, the response is dominated by a single peak at the resonant frequency of 1.7 kHz. The maximum peak velocity recorded was 35 m/s for Orifice 1 and 38 m/s for Orifice 2 at 1.7 kHz.

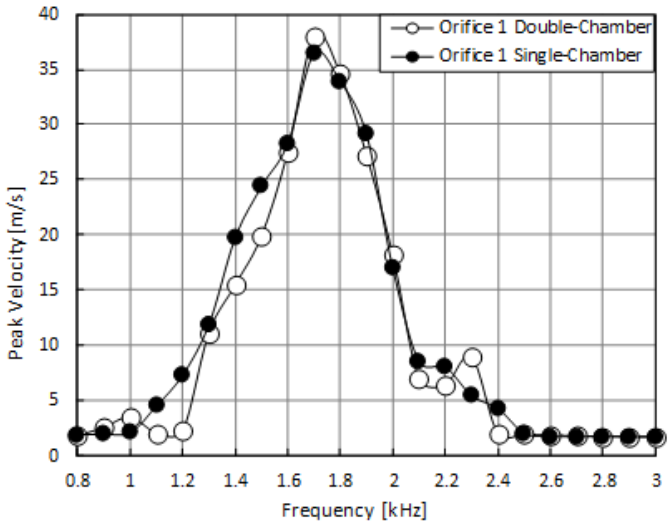

Figure 9. Comparison between round orifice single- and double-chamber SJAs at V_{pp} = 100 V

(a)

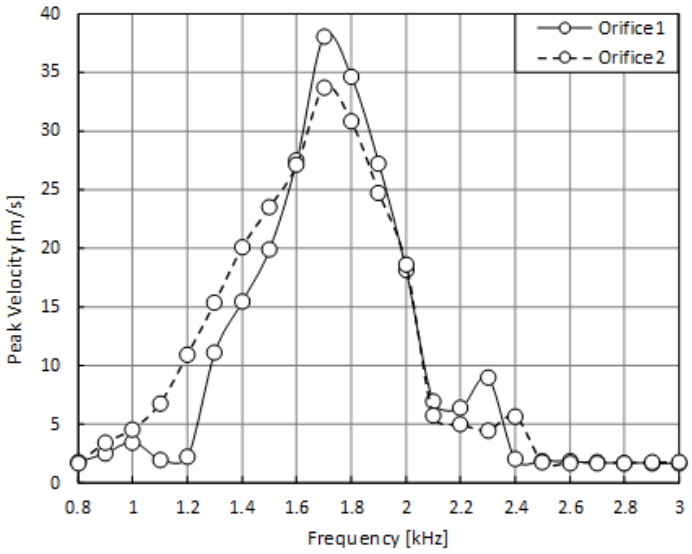

(b)

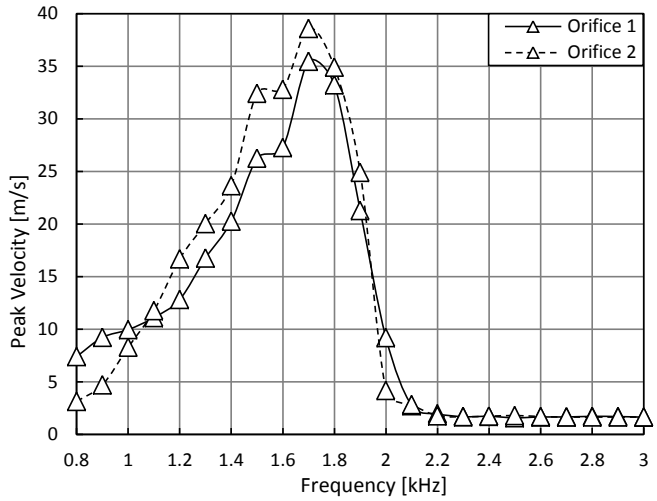

Figure 10. Comparison between orifice shapes in the double-chamber SJA configurations at V_{pp} = 100 V: (a) round orifice; (b) lobed orifice.

Figure 11 summarise the Orifice 1 peak exit velocities of each orifice shape as a function of excitation frequency. It is observed that the round orifice has the maximum peak velocity output (38.0 m/s). However, the maximum peak velocity from the lobed orifice, at 35.5 m/s, is still very close to the round orifice. For both orifice shapes, the resonant frequency occured at 1.7 kHz.

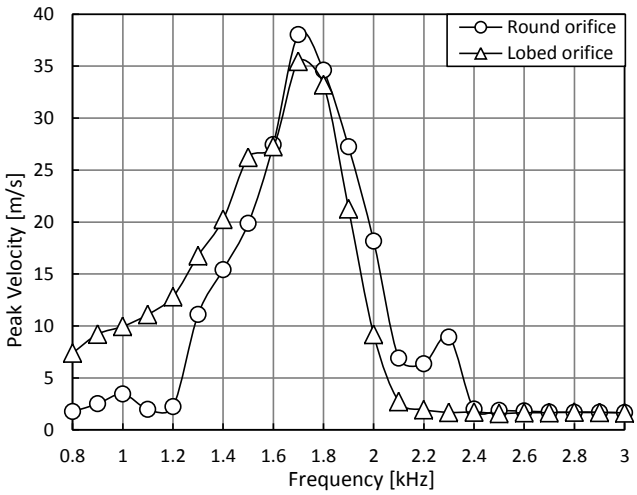

Figure 11. Peak jet velocity comparison of orifice shapes in the double-chamber SJA at V_{pp} = 100 V

A SJA device has two characteristic resonance frequencies, which are related to the theoretical Helmholtz resonance frequency and the diaphragm mechanical resonance frequency. It is observed that the frequency response of the SJA for both orifice shapes is dominated by a single peak at 1.7 kHz, which correlates closely to the theoretical value of diaphragm resonance ($0.87f_D$). It should be noted that previous studies [29], [30], [31], [32] have reported similar results, i.e. a single peak in the frequency response. All of the aforementioned studies reported the lower frequency peak associated with Helmholtz resonance to be missing due to heavy damping. This is attributed to the frequency-dependent non-linear orifice resistance term, which has a larger effect at lower frequencies. It is thus likely in the present results that the lower frequency peak associated with the Helmholtz resonance (812 Hz) has

been heavily damped. Like the findings of Gallas *et al.* [29], a higher frequency peak beyond the dominant peak is observed; at 2.3 kHz in the present results for the round orifice SJA. This is attributable to a harmonic of the resonance frequency of the piezoelectric diaphragm [29].

To verify whether the velocity peak associated with the Helmholtz resonance has been damped, the lumped element method (LEM) was used to model the SJA using MATLAB-Simscape. Figure 12 shows the frequency response as a function of orifice loss coefficient, K, from the SJA LEM model. For lower orifice damping (K=0.4), a lower frequency peak is clearly evident at 800 Hz, which correlates closely to the theoretical value of Helmholtz resonance ($0.98f_H$). For increased orifice damping (K=1.2), the lower frequency peak is completely damped while the higher frequency peak at 2.1 kHz associated with diaphragm resonance ($1.07f_D$) remains undiminished.

The shape of the graph for K=1.2 matches reasonably well to the present experimental results with a couple of exceptions. Firstly, as the LEM model does not account for structural non-linearities or higher-order vibration modes it is not able to capture the peak in the experimental results at 2.3 kHz – similar to the results of Gallas *et al.* [29]. Secondly, compared to the peak associated with diaphragm resonance in the experiment (1.7 kHz; $0.87f_D$) there is a rightward shift of the peak in the LEM model (2.1 kHz; $1.07f_D$). This would suggest that the degree of diaphragm clamping in the SJA, marked by the value of k^2 in Table 2, is not as high as expected. This is likely due to the design of the SJA which is such that the lip does not extend fully around Cavity 2 (Fig. 3b). Hence the compressive load on the diaphragm would be relatively less in the small region where the lip is absent. This lower degree of clamping would also account for the lower Q factor of the experimental peak – a value of 3.4 for both round and lobed orifices compared with 6.1 for the LEM model.

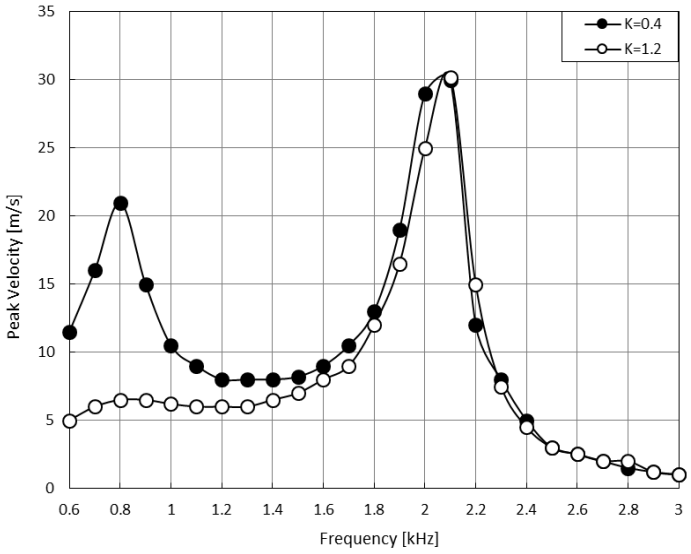

Figure 12. Sensitivity of the actuator output to the orifice loss coefficient, K, in the SJA LEM model

3.2 Power Conversion Efficiency

Figure 13a shows the electrical-to-fluidic power conversion efficiency of the round orifice SJA configuration at 100 and 200 V_{pp}. Efficiency varies from 0 to 15% at 100 V_{pp} and from 0 to 8% at 200 V_{pp}. The SJA is most efficient when it is operated around the SJA resonant frequency of 1.7 kHz for both voltage amplitudes, coinciding with the peak exit velocity. Between 100 V_{pp} and 200 V_{pp}, the peak exit velocity increased by 17% (~8 m/s). The efficiency indicates that at 200 V_{pp} the jets output higher fluidic power, but as a consequence of consuming significantly more electrical power. A reasonable explanation for this behaviour is due to dielectric saturation of the piezoelectric disc [37], which sees a reduction in efficiency as the PZT saturation limit is reached for high voltages (note: the maximum nominal operating voltage for this diaphragm is 30 V_{pp}). Figure 13b presents the efficiency of the lobed orifice at 100 and 200 V_{pp}. Similar to the round orifice, the efficiency at both driving voltages follows the same trend. A peak efficiency of around 12.5% is obtained for 100 V_{pp} at the resonant frequency. When the input voltage is increased to 200 V_{pp}, the peak efficiency is reduced by 2%, although above 2.4 kHz the difference is minimal.

This is due to the fact that the electrical power input is solely converted into mechanical vibration of the diaphragm and heat loss. The velocity output at those high frequencies is zero and therefore no fluidic power is generated.

Finally, it should be noted that the electrical-to-fluid power conversion efficiency of the double-chamber SJA is approximately double that of the single-chamber SJA (~8%); the single-chamber value being similar to those reported for SJAs with brass diaphragms [21], [37]. This doubling of efficiency is due to the SJAs in the double-chamber configuration sharing the same diaphragm with double the number of orifices each generating approximately the same fluid output power as a single-chamber SJA orifice.

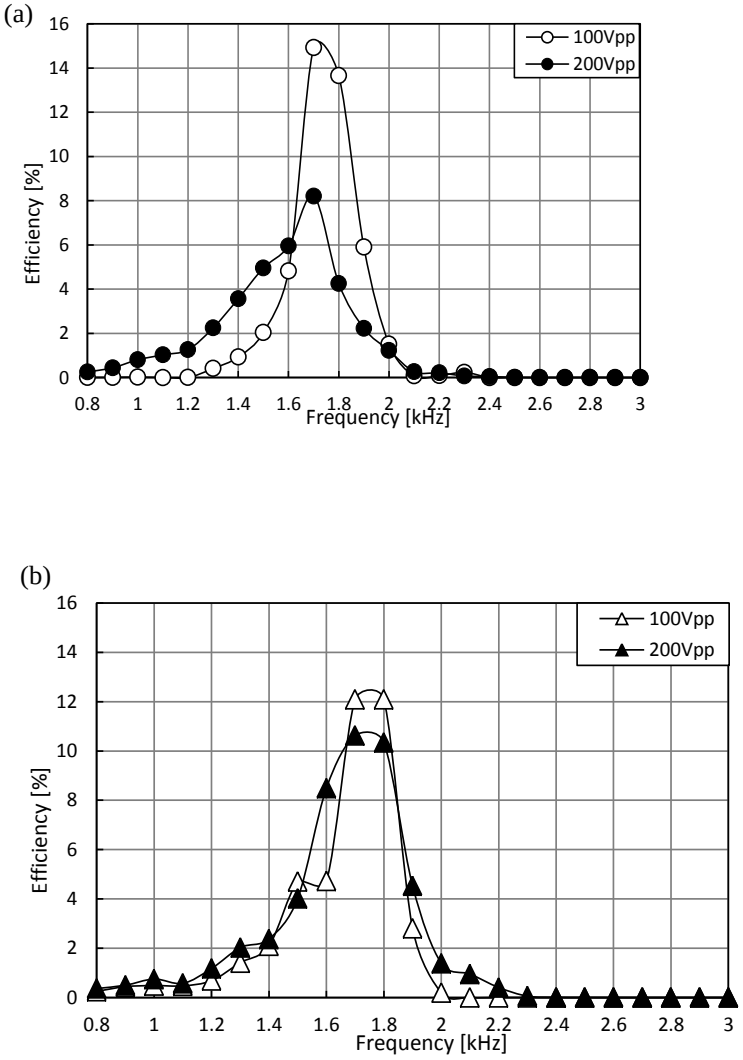

Figure 13. Power conversion efficiency comparison of orifice shapes in the double-chamber SJA: (a) round orifice; (b) lobed orifice

3.3 Noise

3.3.1 Single- and double-chamber comparisons

In order to measure the extent of anti-phase noise reduction the SJA was tested as a double-chamber actuator, with the tests repeated with one of the orifices blocked with tape to simulate a single-chamber actuator. Figures 14a and 14b present the noise output of the SJA for single and double-chamber configuration of the round and lobed

orifice plates respectively. It can be observed in both cases the single-chamber SJA has a louder noise output than the double-chamber configuration. This phenomenon, which is similarly noticed in both orifice plate designs, suggests that there is an anti-phase effect. Part of the overall synthetic jet noise is suppressed because the two orifices in the double-chamber configuration act as a dipole source. Thus the sound produced by the two exhaled jets have 180 degrees phase difference which partially cancel each other out. Moreover, the noise output does not correlate with the jet velocity. The SPL trend in both orifice designs is generally the same. The noise gradually increases as the excitation frequency is increased up to the point where the maximum noise output level is achieved (2.0–2.2 kHz). Note that the frequency at which the SJA produces maximum SPL is the same for both double and single-chamber configurations.

The double chamber SJA with round orifices (Fig. 14a) has an average noise reduction of 9% across the range of frequencies tested. It can also be seen that the maximum noise output is approximately 68 dB and 61 dB for single and double chamber SJAs respectively at 2.0 kHz. The SPL steadily decreases for higher frequencies. At the SJA resonant frequency of 1.7 kHz the noise reduction caused by anti-phase is 3%. The average effect of anti-phase on the lobed orifice SJA is a 5% noise reduction (Fig. 14b). The maximum noise output of 67 dB is seen at 2.2 kHz for both actuator configurations. At the SJA resonant frequency, the noise difference between the single and double chamber actuator is 8%.

3.3.2 Orifice shape comparisons

The aim of this section is to evaluate the impact of the different orifice shapes on the noise output of the double-chamber SJA. Figure 15 shows that both orifice plates generate noise gradually at low frequencies up to 1.6 kHz. Thereafter, there is a sudden increase of SPL about the SJA resonant frequency (1.7 kHz) and beyond to 1.9 kHz. It is observed that the round orifice SJA has a higher noise output than the lobed orifice SJA for frequencies 1.1–2.0 kHz, with the lobed orifice generating higher noise output at excitation frequencies beyond 2.0 kHz. The peak velocity, U_{peak}, of both configurations is at the resonant frequency with the velocity reducing to $0.7U_{peak}$ at 1.6 and 1.9 kHz. The desired operating frequency of the actuator is therefore in the range 1.6–1.9 kHz, as denoted by the dashed lines in Fig. 15. In this range the lobed orifice produces lower noise output than the round orifice, where the lowest noise output is 40 dB at 1.6 kHz. The maximum noise reduction is observed at the resonant frequency where the lobed orifice suppresses noise by 24% relative to the round orifice.

(a)

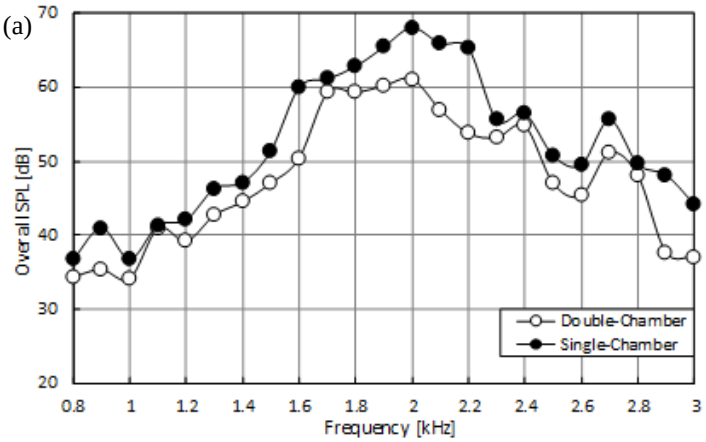

(b)

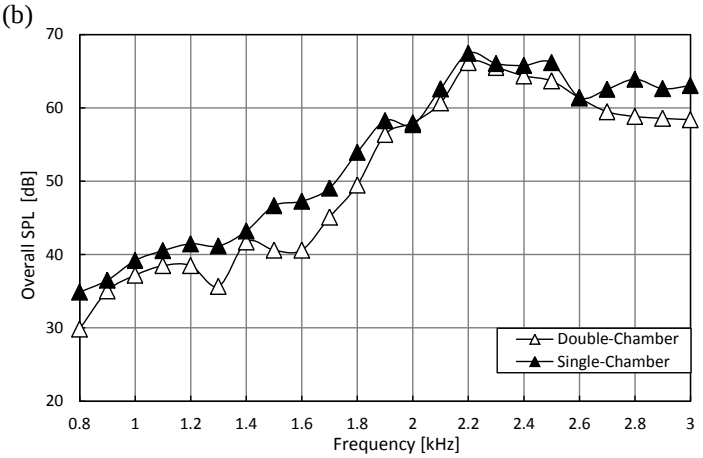

Figure 14. Noise output comparison of single- and double-chamber SJAs at V_{pp} = 100 V: (a) round orifice; (b) lobed orifice

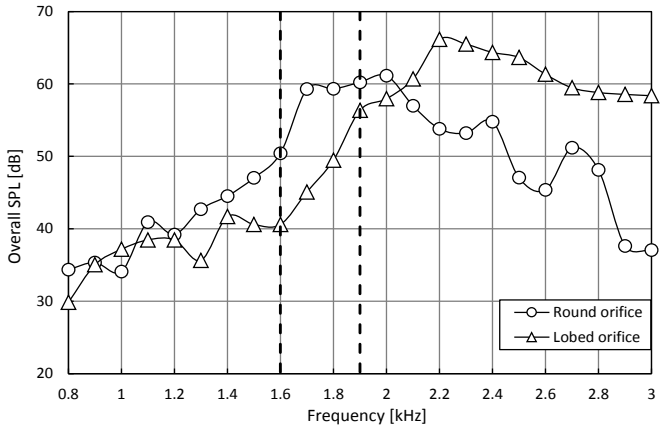

Figure 15. Noise output comparison of round and lobed orifices in the double-chamber SJA at V_{pp} = 100 V. Region between dashed lines indicates desired SJA operating frequency range for peak jet velocity

4 Conclusions

This paper has documented the design and development of piezoelectrical-driven synthetic jet actuator (SJA) with the aim of delivering a reduction in overall SJA noise output while maintaining peak jet velocity output. Hardware development included the use of double-chamber or 'back-to-back' SJAs to reduce noise via anti-phase effect and lobed orifices to reduce noise via intensified jet flow mixing. The experimental work consisted of hot-wire anemometry and microphone recordings to conduct peak jet velocity and noise measurements respectively. Measurements were compared with a baseline SJA (single chamber, round orifice) across a range of actuator excitation frequencies (0.8–3.0 kHz) for a fixed peak-to-peak drive voltage (100 V_{pp}).

Specific conclusions from the experimental work are as follows:

1. For all cases a single velocity peak, U_{peak}, is generated at the SJA resonant frequency of 1.7 kHz, which corresponds closely to the theoretical value of diaphragm resonance ($0.87f_D$).
2. Compared with a single-chamber SJA, a double-chamber SJA reduces actuator noise by up to 8% (4 dB) at the resonant frequency and as much as 10 dB at 1.6 kHz ($0.7U_{peak}$). The peak velocities of both single- and double-chamber SJAs are also the same at U_{peak}=38 m/s. The fact that the peak velocity is the same also illustrates that in the double-chamber configuration the two orifices, which are separated by a distance of 5 orifice diameters (5 mm), do not have fluid interaction with each other that causes jet velocity to be diminished.

3. The use of a lobed orifice reduces actuator noise by up to 15 dB at the resonant frequency compared with a round orifice of the same discharge area in the double-chamber configuration. The peak velocity of the lobed orifice SJA was reduced by 7% (~3 m/s) to 35 m/s, compared with the round orifice.
4. At the resonant frequency an overall SPL reduction of 26% (16 dB) was attained with a double-chamber, lobed orifice SJA (45 dB) compared with a single-chamber, round orifice SJA (61 dB). The maximum noise reduction between these two cases was 32% or 20 dB (40 dB and 60 dB respectively) at 1.6 kHz ($0.7U_{peak}$).
5. The electrical-to-fluidic power conversion efficiency of the double-chamber SJA is approximately 15% at the resonant frequency for round and lobed orifices. This efficiency is double that of the single-chamber SJA (~8%), due to the SJAs in the double-chamber configuration sharing the same diaphragm with double the number of orifices each generating approximately the same fluid output power as a single-chamber SJA orifice.

This work has demonstrated substantial reduction of SJA noise output by methods – namely chamber configuration and orifice shape, that are conducive and feasible for industrial aircraft applications. Further work is required to understand the relative contributions of diaphragm and jet noise and to optimize SJA design (chamber depth; lobe shape, number and amplitude) in order to maximize the level of noise reduction that can be achieved.

Acknowledgements

Thanks are extended to Stephanos Kykkotis for providing the raw hot-wire anemometry and microphone data.

References

[1] A. Glezer, Some aspects of aerodynamic flow control using synthetic-jet actuation, Phil. Trans. R. Soc. A 369 (2011) 1476-1494.
[2] N. Rathay, M.J. Boucher, M. Amitay, E. Whalen, Performance enhancement of a vertical tail using synthetic jet actuators, AIAA J. 52 (2014) 810-820.
[3] M. Arik, An investigation into feasibility of impingement heat transfer and acoustic abatement of meso scale synthetic jets, Appl. Therm. Eng. 27 (2007) 1483-1494.
[4] C.J.M. Lasance, R.M. Aarts, O. Ouweltjes, Synthetic jet cooling part II: Experimental results of an acoustic dipole cooler, Proc. 24th IEEE SEMITHERM Symp., San Jose, CA (2008) 26-31.
[5] C.J.M. Lasance, C. Nicole, R.M. Aarts, O. Ouweltjes, G. Kooijman, J. Nieuwendijk, Synthetic jet cooling using asymmetric acoustic dipoles, Proc. 25th IEEE SEMITHERM Symp., San Jose, CA (2009) 254-260.
[6] U.S. Bhapkar, A. Srivastava, A. Agrawal, Acoustic and heat transfer aspects of an inclined impinging synthetic jet, Intl. J. Therm. Sci. 74 (2013) 145-155.
[7] U.S. Bhapkar, A. Srivastava, A. Agrawal, Acoustic and heat transfer characteristics of an impinging elliptical synthetic jet generated by acoustic actuator, Intl. J. Heat Mass Transfer 79 (2014) 12-23.
[8] L.D. Mangate, M.B. Chaudhari, Heat transfer and acoustic study of impinging synthetic jet using diamond and oval shape orifice, Intl. J. Therm. Sci. 89 (2015) 100-109.
[9] C.S. Greco, A. Ianiro, T. Astarita, G. Cardone, On the near field of single and twin circular synthetic jets, Intl. J. Heat Fluid Flow 44 (2013) 41-52.
[10] A. Önder, J. Meyers, Modification of vortex dynamics and transport properties of transitional axisymmetric jets using zero-net-mass-flux actuation, Phys. Fluids 26 (2014) 075103-1-075103-23.
[11] D.F. Anderson, M. Bratos-Anderson, Noise: Its Measurement, Analysis, Rating and Control, first ed., Avebury Technical, Hampshire, 1993.
[12] F. Lin, M.P. Schoen, R. Sekhri, B. Ramkumar, Modeling acoustic/structural interaction of synthetic jet actuators, J. Vib. Control 16 (2010) 1393-1414.
[13] D.A. Bies, C.H. Hansen, Engineering Noise Control. Theory and Practice, second ed., E & FN Spon, New York, 1996.
[14] D.A. Russell, J.P. Titlow, Y.J. Bemmen, Acoustic monopoles, dipoles and quadrupoles: An experiment revisited, Am. J. Phys. 67 (1999) 660-664.
[15] V.F. Kopiev, M.Y. Zaytsev, N.N. Ostrikov, Subsonic jet noise suppression by a corrugated nozzle, Acoust. Phys. 59 (2013) 207-209.
[16] Bargsten, C.J., and Gibson, M.T. "NASA Innovation in Aeronautics: Select Technologies That Have Shaped Modern Aviation," *American Society for Engineering* Education, NASA Technical Report, Washington DC, 2011.
[17] P. Tide, K. Srinivasan, Effect of chevron count and penetration on the acoustic characteristics of chevron nozzles, Appl. Acoust. 71 (2010) 201-220.
[18] N.K. Depuru Mohan, K.R. Prakash, N.R. Panchapakesan, Mixing augmentation by multiple lobed jets, Am. J. Fluid Dynamics 5 (2015) 55-64.
[19] C.M. Crispo, C.S. Greco, F. Avallone, G. Cardone, On the flow organization of a chevron synthetic jet, Exp. Therm. Fluid Sci. 82 (2017) 136-146.
[20] I. Nastase, A. Meslem, Passive control of jet flows using lobed nozzle geometries, Mécanique Ind. 8 (2007) 101-109.

[21] W.J. Crowther, L.T. Gomes, An evaluation of the mass and power scaling of synthetic jet actuator flow control technology for civil transport aircraft applications, Proc. IMechE. Part I: J. Syst. Control Eng. 222 (2008) 357-372.
[22] M. Jabbal, S. Liddle, J. Potts, W. Crowther, Development of design methodology for a synthetic jet actuator array for flow separation control applications, Proc. IMechE. Part G: J. Aerosp. Eng. 227 (2013) 110-124.
[23] M. Jabbal, S.C. Liddle, W.J. Crowther, Active flow control systems architectures for civil transport aircraft, J. Aircr. 47 (2010) 1966-1981.
[24] L.D. Gomes, W.J. Crowther, N.J. Wood, Towards a practical piezoceramic diaphragm based synthetic jet actuator for high subsonic applications – effect of chamber and orifice depth on actuator peak velocity, Proc. 3rd AIAA Flow Control Conf., AIAA 2006-2859, San Francisco, CA, 5-8 June 2006.
[25] M. Jain, B. Puranik, A. Agrawal, A numerical investigation of effects of cavity and orifice parameters on the characteristics of a synthetic jet flow, Sens. Actuators A: Phys. 165 (2011) 351-366.
[26] G. Godard, M. Stanislas, Control of a decelerating boundary layer. Part 1: optimisation of passive vortex generators, Aerosp. Sci. Technol. 10 (2006) 181-191.
[27] G. Godard, M. Stanislas, Control of a decelerating boundary layer. Part 3: optimisation of round jets vortex generators, Aerosp. Sci. Technol. 10 (2006) 455-464.
[28]W.J. Crowther, Control of separation on a trailing edge flap using air jet vortex generators, J. Aircr. 43 (2006) 1589-1593.
[29] Q. Gallas, R. Holman, T. Nishida, B. Carroll, M. Sheplak, L. Cattafesta, Lumped element modeling of piezoelectrical-driven synthetic jet actuators, AIAA J. 41 (2003) 240-247.
[30] R.N. Sharma, Fluid-dynamics-based analytical model for synthetic jet actuation, AIAA J. 45 (2007) 1841-1847.
[31] T. Persoons, General reduced-order model to design and operate synthetic jet actuators, AIAA J. 50 (2012) 916-927.
[32] L. de Luca, M. Girfoglio, G. Coppola, Modeling and experimental validation of the frequency response of synthetic jet actuators, AIAA J. 52 (2014) 1733-1748.
[33] K.P. Flynn, R.L. Panton, The interaction of Helmholtz resonators in a row when excited by a turbulent boundary layer, J. Acoust. Soc. Am. 87 (1990) 1482-1488.
[34] R.D. Belvins, Formulas for Natural Frequency and Mode Shape, second ed., Von Nostrand Reinhold Company, New York, 1979.
[35] R. Li, R. Sharma, M. Arik, Energy conversion efficiency of synthetic jets, Proc. ASME Pac. Rim Tech. Conf. Exhib. Packag. Integr. Electron. Photonic Syst., MEMS and NEMS, InterPACK (2011) 1-8.
[36] K. Viswanathan, Instrument considerations for accurate jet noise measurements, AIAA J. 44 (2006) 1137-1149.
[37] M. Girfoglio, C.S. Greco, M. Chiatto, L. de Luca, Modeling of efficiency of synthetic jet actuators, Sens. Actuators A: Phys. 233 (2015) 512-521.